

ARTICLE

Received 14 Aug 2014 | Accepted 26 Nov 2014 | Published 6 Jan 2015

DOI: 10.1038/ncomms6955

OPEN

# A ferromagnetically coupled Fe<sub>42</sub> cyanide-bridged nanocage

Soonchul Kang<sup>1</sup>, Hui Zheng<sup>2</sup>, Tao Liu<sup>2</sup>, Kohei Hamachi<sup>1</sup>, Shinji Kanegawa<sup>1</sup>, Kunihisa Sugimoto<sup>3</sup>, Yoshihito Shiota<sup>1</sup>, Shinya Hayami<sup>4</sup>, Masaki Mito<sup>5</sup>, Tetsuya Nakamura<sup>3</sup>, Motohiro Nakano<sup>6</sup>, Michael L. Baker<sup>7</sup>, Hiroyuki Nojiri<sup>7</sup>, Kazunari Yoshizawa<sup>1</sup>, Chunying Duan<sup>2</sup> & Osamu Sato<sup>1</sup>

Self-assembly of artificial nanoscale units into superstructures is a prevalent topic in science. In biomimicry, scientists attempt to develop artificial self-assembled nanoarchitectures. However, despite extensive efforts, the preparation of nanoarchitectures with superior physical properties remains a challenge. For example, one of the major topics in the field of molecular magnetism is the development of high-spin (HS) molecules. Here, we report a cyanide-bridged magnetic nanocage composed of 18 HS iron(III) ions and 24 low-spin iron(II) ions. The magnetic iron(III) centres are ferromagnetically coupled, yielding the highest ground-state spin number ( $S = 45$ ) of any molecule reported to date.

<sup>1</sup>Institute for Materials Chemistry and Engineering, Kyushu University, 6-1 Kasuga-koen, Kasuga, Fukuoka 816-8580, Japan. <sup>2</sup>State Key Laboratory of Fine Chemicals, Dalian University of Technology, 2 Linggong Road, 116024 Dalian, China. <sup>3</sup>Japan Synchrotron Radiation Research Institute, 1-1-1, Kouto, Sayo-cho, Sayo-gun, Hyogo 679-5198, Japan. <sup>4</sup>Graduate School of Science and Technology, Kumamoto University, 2-39-1 Kurokami, Kumamoto 860-8555, Japan. <sup>5</sup>Faculty of Engineering, Kyushu Institute of Technology, Kitakyushu 804-8550, Japan. <sup>6</sup>Research Center for Structural Thermodynamics, Graduate School of Science, Osaka University, Toyonaka, Osaka 560-0043, Japan. <sup>7</sup>Institute for Materials Research, Tohoku University, Katahira 2-1-1, Sendai 980-8577, Japan. Correspondence and requests for materials should be addressed to T.L. (email: liutao@dlut.edu.cn) or to O.S. (email: sato@cm.kyushu-u.ac.jp).

Self-assembled highly symmetric nanostructures are commonplace in nature: for example, the icosahedra of virus capsids and the cuboctahedra of magnetite nanocrystals in magnetotactic bacteria. Following nature's lead, attempts to prepare self-assembled discrete molecular architectures constructed through the coordination of metal ions and organic ligands such as metal–organic polyhedra have captivated many scientists' attention<sup>1–10</sup>. The unique structural and electronic configurations, resulting from the combined features of both metal ions and organic molecules, can give way to diverse functional properties for many applications, such as molecular flasks<sup>11</sup>, catalysis<sup>12</sup>, ion channels<sup>13</sup>, sensors<sup>14</sup>, drug delivery systems<sup>15</sup>, nanomagnets<sup>16–18</sup> including prototypes for quantum information processing<sup>19,20</sup> and gas storage devices<sup>21–24</sup>.

One of the challenges in the field of molecular magnetism is to synthetically prepare new nanoarchitectures with high-ground state spin numbers. To date, numerous high-spin (HS) molecules have been reported<sup>25,26</sup>. Here, we report a giant-spin nanocage that contains 18 HS ferromagnetically coupled Fe<sup>III</sup> ( $S = 5/2$ ) ions resulting in a molecular ground state spin of  $S = 45$ , the largest value known to date<sup>27</sup>. This nanoarchitecture is a mixed valent HS and low-spin (LS) cyano-bridged Fe<sup>III-HS</sup><sub>18</sub>Fe<sup>II-LS</sup><sub>24</sub> compound, structured as a supramolecular cage with a nanometre-sized inner cavity space.

## Results

**Preparation of Fe<sub>42</sub> cyanide-bridged nanocage.** The strategy used to construct the magnetic nanocage is based on the preparation of metal–organic polyhedra<sup>28</sup>. We used metal–organic complexes as building blocks, which not only act as caps but also contain metal centres and cyano groups that enable the introduction of magnetic interactions. Namely, instead of organic tridentate pyridyl ligands, which can provide a large hollow polyhedral structure, we used monoanionic complex ligand {Fe(Tp)(CN)<sub>3</sub>}<sup>−</sup> (Tp = hydrotris(pyrazolyl)borate) units<sup>29–31</sup> as a trinucleating ligand of the metal ions for constructing magnetic nanocage. In addition, the choice of counter metal ions in these structures importantly enables the adjustment of their magnetic properties, facilitating the creation of HS ground states. We employed iron ions in consideration of the magnetic interaction and redox activity of the ferromagnetic metal–cyanide compound: Prussian blue Fe<sup>III</sup><sub>4</sub>[Fe<sup>II</sup>(CN)<sub>6</sub>]<sub>3</sub> · xH<sub>2</sub>O (refs 16,32). The reaction of Fe(CF<sub>3</sub>SO<sub>3</sub>)<sub>2</sub>, 1,3-di(4-pyridyl)propane (dpp), L-ascorbic acid and Li[Fe(Tp)(CN)<sub>3</sub>] in H<sub>2</sub>O led to the isolation of a new [Fe<sup>III</sup><sub>18</sub>Fe<sup>II</sup><sub>24</sub>] spin nanocage: [{Fe(Tp)(CN)<sub>3</sub>}]<sub>24</sub>{Fe(H<sub>2</sub>O)<sub>2</sub>}]<sub>6</sub>{Fe(dpp)(H<sub>2</sub>O)}<sub>12</sub>(CF<sub>3</sub>SO<sub>3</sub>)<sub>6</sub> · 18H<sub>2</sub>O (**1** · 18H<sub>2</sub>O) as green cubic crystals (Supplementary Fig. 1), where **1** contains 42 iron ions, the largest number of metal centres in any cyano-bridged cluster reported to date<sup>33</sup>.

**Characterization of Fe<sub>42</sub> cyanide-bridged nanocage.** Crystallographic analysis of **1** · 18H<sub>2</sub>O reveals that each octahedral {Fe(Tp)(CN)<sub>3</sub>} unit is connected to three Fe ions by three cyanide anions. The Fe ions are further ligated by water and dpp to give octahedral {Fe(NC)<sub>4</sub>(H<sub>2</sub>O)<sub>2</sub>} and {Fe(NC)<sub>4</sub>(dpp)(H<sub>2</sub>O)} coordination spheres, where the Fe centres are in a weakly distorted octahedral environment with axial water molecules (Fig. 1 and Supplementary Tables 1–3). Thus, 24 {Fe(Tp)(CN)<sub>3</sub>}, 12 {Fe(NC)<sub>4</sub>(dpp)(H<sub>2</sub>O)} and 6 {Fe(NC)<sub>4</sub>(H<sub>2</sub>O)<sub>2</sub>} building units are symmetrically disposed in an O space around a central point providing the cube cage, with a separation of 1.96 nm between the most distant Fe ions. Six severely disordered, charge-balancing trifluoromethanesulfonate anions are apparent outside the cationic [Fe<sub>42</sub>]<sup>6+</sup> nanocages, keeping them well separated, and 18 solvent water molecules are located inside the cage.

The <sup>57</sup>Fe Mössbauer spectrum measured for **1** · 18H<sub>2</sub>O at 298 K can be deconvoluted into two doublets exhibiting quadrupole splitting (LS-Fe<sup>II</sup>:  $\delta$  (isomer shift) = 0.065 mm s<sup>−1</sup>,  $\Delta$  (quadrupole splitting) = 0.47 mm s<sup>−1</sup>; HS-Fe<sup>III</sup>:  $\delta$  = 0.43 mm s<sup>−1</sup> and  $\Delta$  = 0.71 mm s<sup>−1</sup>) in a relative intensity ratio of Fe<sup>II</sup>/Fe<sup>III</sup> = 0.55/0.45 (Supplementary Fig. 2 and Supplementary Table 4). Charge considerations and Mössbauer spectroscopic measurements suggest that **1** · 18H<sub>2</sub>O has 24 Fe<sup>II-LS</sup> ions, to which the cyanide carbon atoms coordinate, and 18 Fe<sup>III-HS</sup> ions at room temperature. Note that **1** · 18H<sub>2</sub>O was prepared using {Fe<sup>III</sup>(Tp)(CN)<sub>3</sub>}<sup>−</sup> as a starting material, where the cyanide carbon atoms are coordinated to Fe<sup>III</sup> ions. Electron transfer from Fe<sup>II</sup> ions to the {Fe<sup>III</sup>(Tp)(CN)<sub>3</sub>}<sup>−</sup> units is, therefore, suggested to occur during the reaction, leading to an Fe<sup>II-LS</sup>–CN–Fe<sup>III-HS</sup> linkage. Further, evidence of this linkage was obtained by synchrotron X-ray absorption spectroscopy (XAS) at the Fe L-edge. Comparison of XAS for **1** · 18H<sub>2</sub>O with variants of the starting material compound, Li[Fe<sup>III-LS</sup>(Tp)(CN)<sub>3</sub>] and K<sub>2</sub>[Fe<sup>II-LS</sup>(Tp)(CN)<sub>3</sub>], infers that the valence composition of the 24 {Fe(Tp)(CN)<sub>3</sub>} is consistent with {Fe<sup>II-LS</sup>(Tp)(CN)<sub>3</sub>}<sup>2−</sup> (See Supplementary Fig. 3, with further details of this measurement).

The most remarkable structural feature of **1** · 18H<sub>2</sub>O is that the 18 Fe<sup>III-HS</sup> ions can be identified as the vertices of a highly symmetric entity shown in Fig. 2. First, 12 Fe<sup>III-HS</sup> centres in {Fe(NC)<sub>4</sub>(dpp)(H<sub>2</sub>O)} units are defined as the vertices of cuboctahedron, all of whose sides have a length of 7.85 Å. Second, six square windows of the cuboctahedron are stellated with 24 isosceles triangles, each with side lengths of 6.83, 6.83 and 7.85 Å, with six vertices defined by Fe<sup>III-HS</sup> ions from {Fe(NC)<sub>4</sub>(H<sub>2</sub>O)<sub>2</sub>} units<sup>34,35</sup>. The Fe<sup>II</sup>–CN–Fe<sup>III</sup> linkage of **1** · 18H<sub>2</sub>O classify it as a Prussian blue analogue<sup>36,37</sup> from the standpoint of its electronic state. Prussian blue analogues exhibit in a molecule-based framework with cyanide-bridging akin to the three-dimensional Prussian blue compound Fe<sup>III</sup><sub>4</sub>[Fe<sup>II</sup>(CN)<sub>6</sub>]<sub>3</sub> · xH<sub>2</sub>O. Prussian blue shows ferromagnetic behaviour with a Curie temperature  $T_c$  of 5.5 ± 0.5 K (ref. 32). The observed ferromagnetism involves a long-range order of the Fe<sup>III</sup> ions. While **1** · 18H<sub>2</sub>O is much more complex than Fe<sup>III</sup><sub>4</sub>[Fe<sup>II</sup>(CN)<sub>6</sub>]<sub>3</sub> · xH<sub>2</sub>O, the cyanide bridging units between the Fe<sup>III</sup> ions are similar. The shortest Fe<sup>III</sup>–Fe<sup>III</sup> distances for Prussian blue and **1** · 18H<sub>2</sub>O are 7.2 Å and 6.8 Å through space and 10.2 Å and 9.9 Å along the Fe<sup>III</sup>–NC–Fe<sup>II</sup>–CN–Fe<sup>III</sup> units, respectively. Accordingly, it is reasonable that the 18 Fe<sup>III-HS</sup> ( $S = 5/2$ ) ions, at the vertices in **1** · 18H<sub>2</sub>O, are coupled ferromagnetically.

## Magnetic properties of Fe<sub>42</sub> cyanide-bridged nanocage.

Figure 3a shows the magnetic properties of a polycrystalline sample of **1** · 18H<sub>2</sub>O under a direct current field of 10 kOe from 300 to 30 K and 100 Oe from 30 to 2 K. It indicates the existence of predominantly ferromagnetic interactions and a resulting giant ground-state spin for **1** · 18H<sub>2</sub>O. At 300 K, the  $\chi_m T$  product is 85.5 cm<sup>3</sup> mol<sup>−1</sup> K, and the data in the range 300–30 K can be fitted to the Curie–Weiss law, yielding  $C = 83.2$  cm<sup>3</sup> mol<sup>−1</sup> K and  $\theta = +6.7$  K. This  $C$  value is consistent with the expectations (78.8 cm<sup>3</sup> mol<sup>−1</sup> K with  $g = 2.0$ ) for 18 uncoupled Fe<sup>III</sup> centres ( $S = 5/2$ ). On cooling, the  $\chi_m T$  value becomes slightly larger with temperature, abruptly increasing to 863 cm<sup>3</sup> mol<sup>−1</sup> K at 2 K (Supplementary Fig. 4). This magnetic behaviour and the positive Weiss constant suggest the existence of dominant ferromagnetic exchange interactions in **1** · 18H<sub>2</sub>O. Figure 3b shows  $\chi^{-1}$  versus the T-plot for various applied fields, which displays an inflection in  $\chi^{-1}$  between 10 and 5 K as excited states depopulate, on further cooling below 5 K the slope starts to become linear again, suggesting that it is just the ground state that is mainly populated,

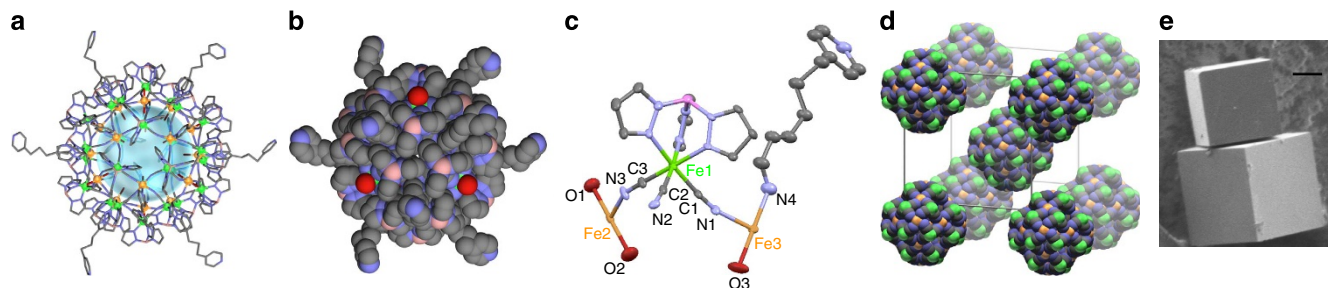


**Figure 1 | Crystal structure of  $1 \cdot 18\text{H}_2\text{O}$ .**  $\text{Fe}^{\text{II}}$  and  $\text{Fe}^{\text{III}}$  ions are shown as light green and orange balls, respectively. **(a)** A framework structure of a single  $[\text{Fe}_{42}]$  nanocage:  $1 \cdot 18\text{H}_2\text{O}$  (14 Å diameter void, blue sphere). All the counter ions ( $\text{CF}_3\text{SO}_3^-$ ) and crystal solvent ( $\text{H}_2\text{O}$ ) are omitted for clarity. **(b)** As in **a**, but as a space-filling model; grey, blue, red, and pink spheres represent C, N, O, and B atoms, respectively. **(c)** The asymmetric unit of  $1 \cdot 18\text{H}_2\text{O}$  with thermal ellipsoids at 30% probability. Hydrogen atoms, counterions and solvent molecules have been omitted for clarity. **(d)** View of the crystal packing for cyano-bridged  $[\text{Fe}_{42}]$  framework. **(e)** Scanning electron microscope image of crystals of compound  $1 \cdot 18\text{H}_2\text{O}$ , illustrating the cubic faces. A scale bar indicates 10  $\mu\text{m}$ .

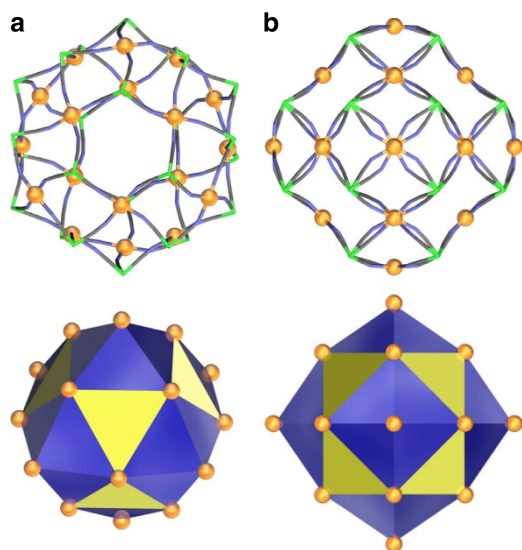


**Figure 2 | Crystal structure of  $\text{Fe}^{\text{III}}$  ions in compound  $1 \cdot 18\text{H}_2\text{O}$ .** Crystal structure looking down through a triangular window **(a)** and a square window **(b)**. A skeleton structure with  $\text{Fe}^{\text{III}}$  atoms (orange balls) bridged by cyano groups of  $1 \cdot 18\text{H}_2\text{O}$  (above). Below each structure,  $\text{Fe}^{\text{III}}$  atoms have been extracted from the crystal structure. Note that the structure of  $1 \cdot 18\text{H}_2\text{O}$  is related to the stellated cuboctahedron structure. However, mathematically defined stellated cuboctahedron is stellated on every triangular face of the cuboctahedron (shown in yellow), whereas in  $1 \cdot 18\text{H}_2\text{O}$  only the square windows are stellated with 24 isosceles triangles (side lengths: 6.83, 6.83 and 7.85 Å).

following the dependence of a paramagnetic  $S = 45$ ,  $g = 2.0$ , spin unit (dot line).

Moreover, the magnetization ( $M$ ) at 2 K (Fig. 3c) rapidly increases at low fields, and then steadily increases with  $H > 15$  kOe to reach a near saturation value of 88.4  $\mu_B$  at 50 kOe, which is in good agreement with the expected value of 90  $\mu_B$  (with  $g = 2.0$ ) for a ground state of  $S_T = 90/2$  (Supplementary Figs 5 and 6). This magnetization behaviour is significantly higher than the Brillouin curve corresponding to 18 non-interacting  $S_{\text{Fe}}$  spins ( $S = 5/2$ , green line), fitting more closely the Brillouin curve for one  $S = 45$  centre (with  $g = 2.0$ , blue line, see Methods). These data support the maximum possible spin state,  $S = 45$ , which is the largest spin ground state number of any molecule ever prepared<sup>27</sup>.

To rule out the possibility of intermolecular interaction or a magnetic ordering between the molecule-based giant spins,

electron paramagnetic resonance (EPR) spectra of  $1 \cdot 18\text{H}_2\text{O}$  have been examined. Figure 3d shows no evidence of intermolecular interaction is present within EPR on decrease of temperature to 1.6 K; the  $g = 2.0$  absorption increases in intensity with no significant variation of line width or shift in resonance field position to evidence intermolecular interactions. No evidence of anisotropy is observed in EPR measurements, it is reasoned that the geometry of the molecular structure of  $1 \cdot 18\text{H}_2\text{O}$  causes the cancelling of single ion anisotropic contributions. In addition, the temperature dependence of magnetization for  $1 \cdot 18\text{H}_2\text{O}$  under various applied magnetic fields does not show evidence of spontaneous magnetization down to 0.5 K (see Supplementary Fig. 7). These results indicate that the cyanide-bridged magnetic  $\text{Fe}_{42}$  nanocage exhibits the maximum spin ground state with isolated molecule  $S = 45$ .

## Discussion

DFT calculations were carried out to estimate changes in the electronic structures of  $1 \cdot 18\text{H}_2\text{O}$ . Calculations were simplified to a cyano-bridged molecular square<sup>38,39</sup> formulated as  $[\text{Fe}^{\text{II}}_2\text{-CN-Fe}^{\text{III}}_2]$  with a  $\text{Tp}^-$  ligand on the  $\text{Fe}^{\text{II}}$  ion, a pyridine ligand, and  $\text{H}_2\text{O}$  on the  $\text{Fe}^{\text{III}}$  ion (Fig. 4, and Supplementary Tables 5–7). Figure 4 shows HS ferromagnetic (HSFM) state was the ground state, and LS ferromagnetic (LSFM) and antiferromagnetic (LSAF) states were above 5.5 kcal mol<sup>-1</sup> and 1.5 kcal mol<sup>-1</sup>, respectively. DFT calculations indicate the ferromagnetic character of a magnetic coupling between the two diagonal  $\text{Fe}^{\text{III-HS}}$  ions in the square framework. The calculated  $J$  value (35.5 cm<sup>-1</sup> at the B3LYP\* level) for the tetranuclear cyano-bridged square complex overestimates the magnitude of the exchange coupling parameters. The overestimation of coupling constants by a factor of 2–4 is not unusual in DFT calculations<sup>40,41</sup>. The calculation predicts the correct sign for  $J$  corresponding to the ferromagnetic nature of the ground state in the  $[\text{Fe}_{42}]$  nanocage.

We have presented a  $\text{Fe}_{42}$  cyanide-bridged nanocage with a HS framework. Many metal–cyanide clusters have been synthesized since the discovery of Prussian blue. Our metal–cyanide polyhedron is the largest cyanide-bridged polynuclear cluster and exhibits a rare hollow structure. Among the various morphologies of nanoarchitectures, hollow spheres are of great interest because of their high surface to volume ratio and large pore volume, which could be exploited for promising applications in the controlled encapsulation and release of molecules.

In summary, we report a new high-nuclearity iron complex with a HS framework. In the  $\text{Fe}_{42}$  cyanide-bridged nanocage,

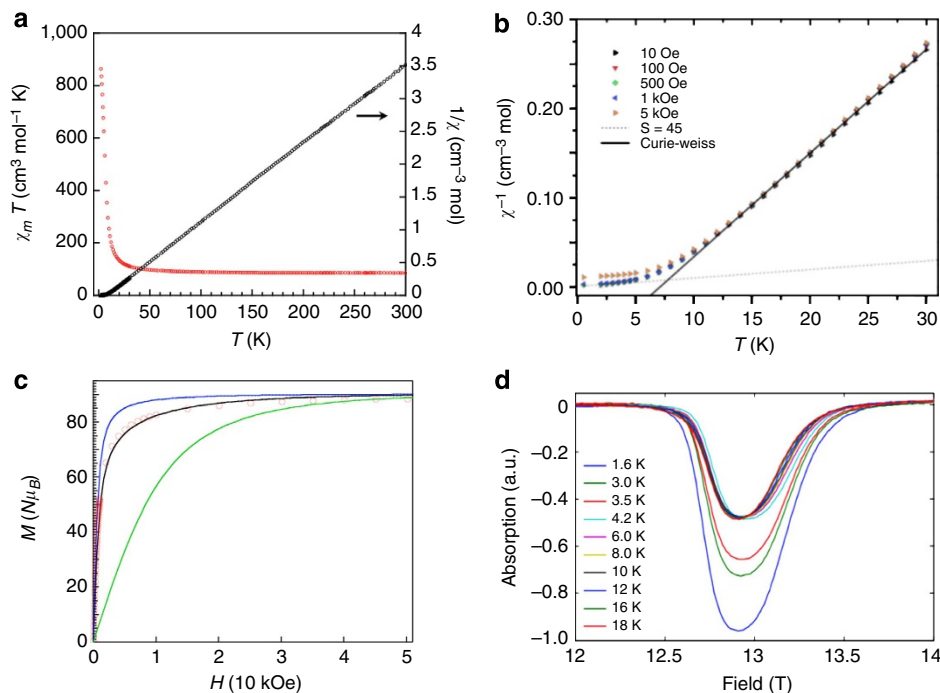


**Figure 3 | Magnetic characteristics for  $1 \cdot 18\text{H}_2\text{O}$ .** (a) Temperature dependence of  $\chi_m T$  and  $\chi_m^{-1}$  for  $1 \cdot 18\text{H}_2\text{O}$  ( $H_{dc} = 100$  Oe from 2 to 30 K and  $H_{dc} = 10,000$  Oe from 30 to 300 K). (b)  $\chi^{-1}$  versus  $T$  for various applied fields. Calculations of susceptibility are represented below 5 K by a paramagnetic  $S = 45$  with a  $g = 2$ , and the Curie-Weiss law above 10 K. (c) Magnetization versus external magnetic field curve for  $1 \cdot 18\text{H}_2\text{O}$  at 2 K. Red circles are experimental data. Blue line corresponds to simulation employing the Brillouin function for  $S = 45$  with  $g = 2.0$ . The green line represents the 18 times value of the Brillouin function that corresponds to  $S = 5/2$  with  $g = 2.0$ . The black line represents the simulation curve described in Methods. (d) The temperature-dependent EPR spectra of  $1 \cdot 18\text{H}_2\text{O}$  (360 GHz continuous wave EPR).

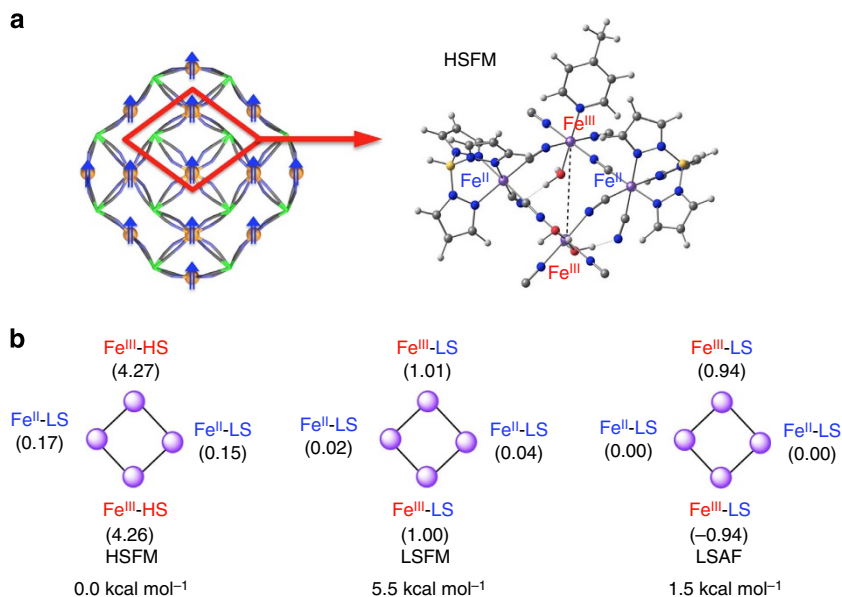


**Figure 4 | DFT calculation.** (a) A skeleton structure of cyano-bridged  $[\text{Fe}_{42}]$  framework.  $\text{Fe}^{\text{II}}$  and  $\text{Fe}^{\text{III}}$  ions are shown as light green and orange balls, respectively. Blue arrows indicate  $\text{Fe}^{\text{III}}$  sites that are ferromagnetically coupled. (b) Optimized geometry of the tetranuclear cyanide-bridged square complex in the HS ferromagnetic (HSFM) state, calculated spin densities, and relative energies of HSFM, LS ferromagnetic (LSFM) state and LS antiferromagnetic (LSAF) state at the B3LYP\* level of theory. Units are in  $\text{kcal mol}^{-1}$ . Computed energies of the tetranuclear cyanide-bridged square complex are  $0.0 \text{ kcal mol}^{-1}$  in the HSFM state (undecet state),  $5.5 \text{ kcal mol}^{-1}$  in the LSFM state (triplet state) and  $1.5 \text{ kcal mol}^{-1}$  in the LSAF state (open-shell singlet state). The HS antiferromagnetic (HSAF) state is not available as a low-lying open-shell singlet state. The distances between the diagonal  $\text{Fe}^{\text{III}}$  atoms are  $6.817 \text{ \AA}$  in the HSFM state and  $6.785 \text{ \AA}$  in the LSFM state.

magnetic metal centres are ferromagnetically coupled, yielding the highest ground state spin number ( $S = 45$ ) of any prepared molecule.

## Methods

**Synthesis of  $\text{Fe}_{42}$  cyanide-bridged nanocage.**  $[\{\text{Fe}(\text{Tp})(\text{CN})_3\}_{24}\{\text{Fe}(\text{H}_2\text{O})_2\}_6]\{\text{Fe}(\text{dpp})(\text{H}_2\text{O})_{12}(\text{CF}_3\text{SO}_3)_6\} \cdot 18\text{H}_2\text{O} : 1 \cdot 18\text{H}_2\text{O}$ .



A 1 ml aqueous solution of 17  $\mu\text{mol}$  of  $\text{Li}[\text{Fe}(\text{Tp})(\text{CN})_3]$  and 8.3  $\mu\text{mol}$  of 1,3-di(4-pyridyl)propane was slowly layered over a 2 ml aqueous solution of 8.3  $\mu\text{mol}$  of  $\text{Fe}(\text{CF}_3\text{SO}_3)_2$  and 1.7  $\mu\text{mol}$  of L-ascorbic acid with  $\text{H}_2\text{O}$  (1 ml) as a middle buffer layer under an aerobic condition. Crystallization required several weeks and gave crystals in 30% yield based on  $\text{Li}[\text{Fe}(\text{Tp})(\text{CN})_3]$ . The crystals were washed with  $\text{H}_2\text{O}$  and dried under reduced pressure for 12 h. As prepared compound, before vacuum drying, has approximately 50  $\text{H}_2\text{O}$  molecules inside the cage (compound **1** · ca 50  $\text{H}_2\text{O}$ ), which become partially desolvated when exposed to air at room temperature. Therefore, the physical measurements performed on compound **1** · 18  $\text{H}_2\text{O}$  were prepared carefully to prevent desolvation. The reported structures have been characterized by the single-crystal X-ray crystallography (Supplementary Tables 1–3 and Supplementary Data 1 and 2).

**Elemental analysis.** Elemental analysis for  $\text{C}_{450}\text{H}_{492}\text{B}_{24}\text{F}_{18}\text{Fe}_{42}\text{N}_{240}\text{O}_{60}\text{S}_6$  (**1** · 18  $\text{H}_2\text{O}$ ) is as follows: calculated (found) C, 40.45 (40.65); H, 3.71 (3.54) and N, 25.16 (25.30). Inductively coupled plasma atomic emission spectroscopy (ICP-AES) analysis was performed to measure the Fe content in the solid sample of **1** · 18  $\text{H}_2\text{O}$ . ICP-AES analysis shows that the Fe contents in **1** · 18  $\text{H}_2\text{O}$  is 16 wt%, which is in good agreement with the calculated value of 16.8 wt%. In addition, analysis of the sulfur content of **1** · 18  $\text{H}_2\text{O}$  with total sulfur analyser (TOX-100) reveals the sulfur content is 1.6 wt% (calcd. 1.4 wt%).

**X-ray structure determination.** Single-crystal synchrotron radiation X-ray diffraction experiments were performed at 295 K for **1** · 18  $\text{H}_2\text{O}$ , and 100 K for **1** · ca 50  $\text{H}_2\text{O}$  using a Rigaku Mercury2 CCD detector at BL02B1/SPRING-8 (Hyogo, Japan). The wavelength of the incident X-ray was 0.6186 or 0.6202 Å. We used anomalous dispersion coefficients for structure refinement,  $f'$  and  $f''$ , in dependence on X-ray energy calculated on the original *FPRIME* code of Cromer.

**SEM measurements.** Scanning electron microscopy studies were performed with a Hitachi Ultra-high Resolution Scanning Electron Microscope SU8000.

**Physical measurements.** Magnetic susceptibility measurements of samples were performed on a Quantum Design SQUID (MPMS XL-5 and MPMS XL-7) magnetometer. To prevent the loss of uncoordinated water molecules, the sample was introduced directly into the sample chamber at 100 K without purging, while flowing He gas. Keep the sample stay at 100 K for several minutes and then purge the chamber. At the end, vent the sample space with He gas and start the measurement. Data were corrected for the diamagnetic contribution calculated from Pascal constants. The Mössbauer spectra (isomer shift versus metallic iron at room temperature) were measured using a Wissel MVT-1000 Mössbauer spectrometer with a  $^{57}\text{Co}/\text{Rh}$  source in the transmission mode. All isomer shifts are given relative to  $\alpha\text{-Fe}$  at room temperature. EPR measurements were performed with the Terahertz ESR Apparatus (TESRA-IMR) installed in the magnetism division of Institute of Materials Research (IMR), Tohoku University. A solenoid magnet is fed by a 90-kJ capacitor bank delivering a field pulse of 25 ms in width. Applied fields from 0 to 30 T were investigated for a range of EPR microwave frequencies from 90 to 405 GHz generated by backward-travelling wave oscillators. Measurements were performed in a He4 cryostat down to 1.6 K.

**Simulation of magnetization process.** The magnetization curve was compared with the mean-field simulation assuming an HDVV (Heisenberg–Dirac–Van Vleck)-type spin Hamiltonian:  $\hat{H} = -2J \sum_{\langle i,j \rangle} \hat{S}_i \cdot \hat{S}_j$ , where a uniform isotropic exchange parameter  $J$  makes all the pair of  $S = 5/2$  spins coupled. This Hamiltonian gives the energy eigenvalues  $E(S_{\text{total}}) = -J \{S_{\text{total}}(S_{\text{total}} + 1) - 18s(s + 1)\}$  with the resultant spin of the molecule  $S_{\text{total}}$ , and the magnetic susceptibility is easily calculated following the Van Vleck formula. The simulation curve with a ferromagnetic coupling  $zJ/k_B = +0.5$  K ( $z = 17$ ) and  $g$  factor of 2.0 agreed well with the experimental values.

**XAS measurements.** X-ray absorption spectra were measured on the soft X-ray undulator beam-line BL25SU at Spring 8, Japan. Soft X-rays circularly polarized from a twin helical undulator were monochromated and focused onto a thin polycrystalline layer of **1** · 18  $\text{H}_2\text{O}$ . The measured sample was fixed with carbon tape to a sapphire sample holder. X-ray absorption spectra were measured by the total electron yield method in which the sample current is directly measured while scanning the photon energy. Measurements were performed at zero applied magnetic field and hence both positive and negative X-ray helices resulted in equivalent absorption spectra. The sample chamber for the soft XAS keeps a high vacuum of  $10^{-5}$  Pa or the better. Measurements of **1** · 18  $\text{H}_2\text{O}$  were repeated incrementally over several days and were found not to exhibit changes in spectral line shape with respect to the time spent under vacuum. Care was taken during XAS measurements to control the effect of photoreduction. The incident beam intensity was incrementally reduced until consistent multiple measurements at the same sample spot were obtained after an intensity reduction to 7%. To ensure damage was not encountered in short time periods, rapid measurements over defined features of the  $L_3$  edge were measured repeatedly and ensured to be coincident.

**DFT calculation.** Full details of computational method are given in the Supplementary Methods.

## References

- Olenyuk, B., Whiteford, J. A., Fechtenkotter, A. & Stang, P. J. Self-assembly of nanoscale cuboctahedra by coordination chemistry. *Nature* **398**, 796–799 (1999).
- Takeda, N., Umamoto, K., Yamaguchi, K. & Fujita, M. A nanometre-sized hexahedral coordination capsule assembled from 24 components. *Nature* **398**, 794–796 (1999).
- O’Keeffe, M. & Yaghi, O. M. Deconstructing the crystal structures of metal-organic frameworks and related materials into their underlying nets. *Chem. Rev.* **112**, 675–702 (2012).
- Sun, Q. F. *et al.* Self-assembled  $M_{24}L_{48}$  polyhedra and their sharp structural switch upon subtle ligand variation. *Science* **328**, 1144–1147 (2010).
- Chichak, K. S. *et al.* Molecular borromean rings. *Science* **304**, 1308–1312 (2004).
- Bunzen, J. *et al.* Self-assembly of  $M_{24}L_{48}$  polyhedra based on empirical prediction. *Angew. Chem. Int. Ed.* **51**, 3161–3163 (2012).
- Tranchemontagne, D. J., Ni, Z., O’Keeffe, M. & Yaghi, O. M. Reticular chemistry of metal-organic polyhedra. *Angew. Chem. Int. Ed.* **47**, 5136–5147 (2008).
- An, J. *et al.* Metal-adeninate vertices for the construction of an exceptionally porous metal-organic framework. *Nat. Commun.* **3**, 604 (2012).
- Liu, Y., Hu, C., Comotti, A. & Ward, M. D. Supramolecular Archimedean cages assembled with 72 hydrogen bonds. *Science* **333**, 436–440 (2011).
- Riddell, I. A. *et al.* Anion-induced reconstitution of a self-assembling system to express a chloride-binding  $\text{Co}_{10}\text{L}_{15}$  pentagonal prism. *Nat. Chem.* **4**, 751–756 (2012).
- Yoshizawa, M., Klosterman, J. K. & Fujita, M. Functional molecular flasks: new properties and reactions within discrete, self-assembled hosts. *Angew. Chem. Int. Ed.* **48**, 3418–3438 (2009).
- Pluth, M. D., Bergman, R. G. & Raymond, K. N. Acid catalysis in basic solution: a supramolecular host promotes orthoformate hydrolysis. *Science* **316**, 85–88 (2007).
- Jung, M., Kim, H., Baek, K. & Kim, K. Synthetic ion channel based on metal-organic polyhedra. *Angew. Chem. Int. Ed.* **47**, 5755–5757 (2008).
- Wang, J., He, C., Wu, P., Wang, J. & Duan, C. An amide-containing metal-organic tetrahedron responding to a spin-trapping reaction in a fluorescent enhancement manner for biological imaging of NO in living cells. *J. Am. Chem. Soc.* **133**, 12402–12405 (2011).
- Wang, H. N. *et al.* Stepwise assembly of metal-organic framework based on a metal-organic polyhedron precursor for drug delivery. *Chem. Commun.* **47**, 7128–7130 (2011).
- Beltran, L. M. & Long, J. R. Directed assembly of metal-cyanide cluster magnets. *Acc. Chem. Res.* **38**, 325–334 (2005).
- Li, D. *et al.* Magnetic and optical bistability driven by thermally and photoinduced intramolecular electron transfer in a molecular cobalt-iron prussian blue analogue. *J. Am. Chem. Soc.* **130**, 252–258 (2008).
- Gatteschi, D., Sessoli, R. & Villain, J. *Molecular nanomagnets* (Oxford Univ. Press, 2006).
- Leuenberger, M. N. & Loss, D. Quantum computing in molecular magnets. *Nature* **410**, 789–793 (2001).
- Troiani, F. *et al.* Molecular engineering of antiferromagnetic rings for quantum computation. *Phys. Rev. Lett.* **94**, 207208 (2005).
- Sudik, A. C. *et al.* Design, synthesis, structure, and gas ( $\text{N}_2$ , Ar,  $\text{CO}_2$ ,  $\text{CH}_4$ , and  $\text{H}_2$ ) sorption properties of porous metal-organic tetrahedral and heterocuboidal polyhedra. *J. Am. Chem. Soc.* **127**, 7110–7118 (2005).
- Duriska, M. B. *et al.* Systematic metal variation and solvent and hydrogen-gas storage in supramolecular nanoballs. *Angew. Chem. Int. Ed.* **48**, 8919–8922 (2009).
- Farha, O. K. *et al.* Metal-organic framework materials with ultrahigh surface areas: is the sky the limit? *J. Am. Chem. Soc.* **134**, 15016–15021 (2012).
- Farha, O. K. *et al.* De novo synthesis of a metal-organic framework material featuring ultrahigh surface area and gas storage capacities. *Nat. Chem.* **2**, 944–948 (2010).
- Launay, J. P. & Verdager, M. *Electrons in Molecules: From Basic Principles to Molecular Electronics* (Oxford Univ. Press, 2013).
- Pedersen, K. S., Bendix, J. & Clérac, R. Single-molecule magnet engineering: building-block approaches. *Chem. Commun.* **50**, 4396–4415 (2014).
- Ako, A. M. *et al.* A ferromagnetically coupled  $\text{Mn}_{19}$  aggregate with a record  $S = 83/2$  ground spin state. *Angew. Chem. Int. Ed.* **45**, 4926–4929 (2006).
- Cook, T. R., Zheng, Y. R. & Stang, P. J. Metal-organic frameworks and self-assembled supramolecular coordination complexes: comparing and contrasting the design, synthesis, and functionality of metal-organic materials. *Chem. Rev.* **113**, 734–777 (2013).
- Lescouezec, R., Vaissermann, J., Lloret, F., Julve, M. & Verdager, M. Ferromagnetic coupling between low- and high-spin iron(III) ions in the

- tetranuclear complex fac-[[Fe<sup>III</sup>[HB(pz)<sub>3</sub>](CN)<sub>2</sub>(μ-CN)]<sub>3</sub>Fe<sup>III</sup>(H<sub>2</sub>O)<sub>3</sub>]\* 6H<sub>2</sub>O ([HB(pz)<sub>3</sub>]<sup>-</sup> = hydrotris(1-pyrazolyl)borate. *Inorg. Chem.* **41**, 5943–5945 (2002).
30. Wang, S. *et al.* [(Tp<sub>8</sub>(H<sub>2</sub>O)<sub>6</sub>Cu(II)<sub>6</sub>Fe(III)<sub>8</sub>(CN)<sub>24</sub>]<sup>4+</sup>: a cyanide-bridged face-centered-cubic cluster with single-molecule-magnet behavior. *Angew. Chem. Int. Ed.* **43**, 5940–5943 (2004).
  31. Wang, S., Ding, X. H., Zuo, J. L., You, X. Z. & Huang, W. Tricyanometalate molecular chemistry: A type of versatile building blocks for the construction of cyano-bridged molecular architectures. *Coord. Chem. Rev.* **255**, 1713–1732 (2011).
  32. Ito, A., Suenaga, M. & Ono, K. Mössbauer study of soluble Prussian blue, insoluble Prussian blue, and Turnbull's blue. *J. Chem. Phys.* **48**, 3597–3599 (1968).
  33. Wang, X. Y., Prosvirin, A. V. & Dunbar, K. R. A dicosanuclear {Mo<sub>8</sub>Mn<sub>14</sub>} cluster based on [Mo(CN)<sub>7</sub>]<sup>4-</sup>. *Angew. Chem. Int. Ed.* **49**, 5081–5084 (2010).
  34. Sun, Q. F., Sato, S. & Fujita, M. An M<sub>18</sub>L<sub>24</sub> stellated cuboctahedron through post-stellation of an M<sub>12</sub>L<sub>24</sub> core. *Nat. Chem.* **4**, 330–333 (2012).
  35. Milway, V. A. *et al.* Directed Synthesis of {Mn<sub>18</sub>Cu<sub>6</sub>} Heterometallic Complexes. *Angew. Chem. Int. Ed.* **52**, 1949–1952 (2013).
  36. Ferlay, S., Mallah, T., Ouahes, R., Veillet, P. & Verdaguer, M. *Nature* **378**, 701–703 (1995).
  37. Hoshino, N. *et al.* Three-way switching in a cyanide-bridged [CoFe] chain. *Nat. Chem.* **4**, 921–926 (2012).
  38. Mondal, A. *et al.* Photomagnetic effect in a cyanide-bridged mixed-valence Fe<sup>II</sup>Fe<sup>III</sup> molecular square. *Chem. Commun.* **48**, 5653–5655 (2012).
  39. Zhang, Y. *et al.* Reversible thermally and photoinduced electron transfer in a cyano-bridged {Fe<sub>2</sub>Co<sub>2</sub>} square complex. *Angew. Chem. Int. Ed.* **49**, 3752–3756 (2010).
  40. Brunold, T. C., Tamura, N., Kitajima, N., Moro-oka, Y. & Solomon, E. I. Spectroscopic study of [Fe<sub>2</sub>(O<sub>2</sub>)(OBz)<sub>2</sub>{HB(pz)<sub>3</sub>}]<sub>2</sub>: nature of the μ-1,2 peroxide – Fe(III) bond and its possible relevance to O<sub>2</sub> activation by non-heme iron enzymes. *J. Am. Chem. Soc.* **120**, 5674–5690 (1998).
  41. Binning, Jr R. C. & Babelo, D. E. High-spin versus broken symmetry—effect of DFT spin density representation on the geometries of three diiron (III) model compounds. *J. Comput. Chem.* **29**, 716–723 (2007).

## Acknowledgements

This work was supported by JSPS KAKENHI Grant Number 25109533, 24109014, 24790061, 26810039 and the Mitsubishi Foundation, and Network Joint Research Center for Materials and Devices, and the NSFC (Grant 21421005, 91122031, 21322103). M.L.B. thanks the JSPS for a post-doctoral fellowship. This work was partly performed as the Inter-university Cooperative Research Program of IMR, Tohoku Univ. This work was

partly supported by Nanotechnology Platform Program (Molecule and Material Synthesis) of the Ministry of Education, Culture, Sports, Science and Technology (MEXT), Japan. The synchrotron radiation experiments were performed at the BL02B1 and BL25SU of SPring-8 with the approval of the Japan Synchrotron Radiation Research Institute (JASRI) (Proposal No. 2012B1582, 2013B1032, and 2013A1127) and at the beam-line BL10 of the SAGA Light Source with the approval of the Kyushu Synchrotron Light Research Center (Proposal No. 1304028PT).

## Author contributions

T.L. and C.D. in Dalian and O.S. in Fukuoka conceived and supervised the project. S. Kang, K.H., S. Kanegawa and H.Z. planned, implemented materials synthesis and characterization and analysed the magnetic measurements data. K.S. finalized the synchrotron X-ray data. Y.S. and K.Y. contributed to the DFT calculation. S.H. performed the Mössbauer measurement. M.N. and M.M. contributed to analyses of the magnetic susceptibility. M.L.B. and H.N. were responsible for experiments performed in large magnetic fields and XAS measurements. T.N. contributed to the XAS experiments. S. Kang, Y.S., L.T. and O.S. wrote the manuscript. All authors discussed the results and commented on the manuscript. S. Kang, and H.Z. contributed to this work equally.

## Additional information

**Accession codes:** The X-ray crystallographic coordinates for structures reported in this Article have been deposited at the Cambridge Crystallographic Data Centre (CCDC), under deposition number CCDC 932131 and 932133. These data can be obtained free of charge from The Cambridge Crystallographic Data Centre via [www.ccdc.cam.ac.uk/data\\_request/cif](http://www.ccdc.cam.ac.uk/data_request/cif).

**Supplementary Information** accompanies this paper at <http://www.nature.com/naturecommunications>

**Competing financial interests:** The authors declare no competing financial interests.

**Reprints and permission** information is available online at <http://npg.nature.com/reprintsandpermissions/>

**How to cite this article:** Kang, S. *et al.* A ferromagnetically coupled Fe<sub>42</sub> cyanide-bridged nanocage. *Nat. Commun.* **6**:5955 doi: 10.1038/ncomms6955 (2015).



This work is licensed under a Creative Commons Attribution 4.0 International License. The images or other third party material in this article are included in the article's Creative Commons license, unless indicated otherwise in the credit line; if the material is not included under the Creative Commons license, users will need to obtain permission from the license holder to reproduce the material. To view a copy of this license, visit <http://creativecommons.org/licenses/by/4.0/>